JACS
JOURNAL OF THE AMERICAN CHEMICAL SOCIETY

ARTICLE

pubs.acs.org/JACS

Controlling Chiral Organization of Molecular Rods on Au(111) by Molecular Design

Martin M. Knudsen,[§] Nataliya Kalashnyk,[‡] Federico Masini,[‡] Jacob R. Cramer,[§] Erik Lægsgaard,[‡] Flemming Besenbacher,[‡] Trolle R. Linderoth,*[,‡] and Kurt V. Gothelf*[,§]

[§]Danish National Research Foundation: Center for DNA Nanotechnology (CDNA), Department of Chemistry and iNANO, Aarhus University, Langelandsgade 140, 8000 Aarhus C, Denmark

[‡]Interdisciplinary Nanoscience Center (iNANO) and Department of Physics and Astronomy, Aarhus University, Ny Munkegade 118, 8000 Aarhus C, Denmark

Supporting Information

ABSTRACT: Chiral self-assembled structures formed from organic molecules adsorbed on surfaces have been the subject of intense investigation in the recent decade, owing both to relevance in applications such as enantiospecific heterogeneous catalysis or chiral separation as well as to fundamental interest, for example, in relation to the origin of biomolecular homochirality. A central target is rational design of molecular building blocks allowing transfer of chirality from the molecular to the supramolecular level. We previously studied the surface self-assembly of a class of linear compounds based on an oligo(phenylene ethynylene) backbone, which were shown to form a characteristic windmill adsorption pattern on the Au(111) surface. However, since these prochiral compounds were intrinsically achiral, domains with oppositely oriented windmill motifs and related conformational surface enantiomers were always realized in equal proportion. Here we report on the enantioselective, high yield chemical synthesis of a structurally related but intrinsically chiral compound in which two peripheral *tert*-butyl substituents are replaced by *sec*-butyl groups, each containing an (*S*) chiral center. Using scanning tunneling microscopy under ultrahigh vacuum conditions, we characterize the adsorption structures formed from this compound on the Au(111) surface. The perturbation introduced by the modified molecular design is found to be sufficiently small so structures form that are closely analogous to those observed for the original *tert*-butyl substituted compound. However, as demonstrated from careful statistical analysis of high-resolution STM images, the introduction of the two chiral (*S*)-*sec*-butyl substituents leads to a strong preference for windmill motifs with one orientation, demonstrating control of the chiral organization of the molecular backbones through rational molecular design.

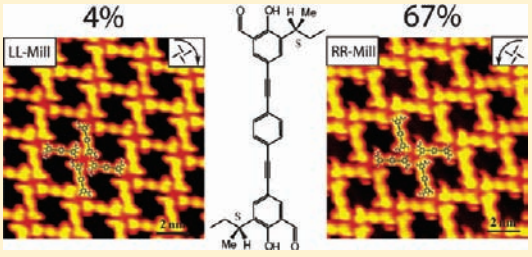

INTRODUCTION

One of the ultimate goals within the very active field of supramolecular self-assembly on surfaces is to be able to obtain desired molecular architectures through rational design of molecular building blocks, providing control over intermolecular and molecule−substrate interaction forces. A large number of studies have focused on characterizing structures formed from organic molecules absorbed on surfaces, not least by the technique of scanning tunneling microscopy (STM), which enables real-space imaging with submolecular resolution, allowing the underlying interactions and assembly principles to be rationalized.[1−7] In a select number of instances, this has resulted in demonstrations of structural control by molecular design,[2] for instance, with respect to dimensionality of self-assembled structures[8] or pore sizes in two-dimensional networks.[9−11] A highly fascinating branch of surface supramolecular chemistry concerns surface chirality,[12−15] which offers particular challenges since not only the structures themselves but also their handedness have to be controlled through exploitation of subtle recognition forces. Molecular chirality on surfaces can be discerned by STM,[16] and chiral adsorption and self-assembly has attracted much attention in the past decade,[17−26] owing both to potential relevance in applications such as heterogeneous asymmetric catalysis,[27−31] enantiomeric separation and chiral sensors as well as to fundamental interest, for example, in relation to the origin of the homochirality of biomolecules.[32,33] One of the most interesting questions within this area concerns how surfaces can be chirally functionalized by transfer of chirality from the molecular to the supra-molecular level through molecular self-assembly. Most obviously, surfaces can be rendered globally homochiral through adsorption of a single enantiomer of an intrinsically chiral molecule.[19] Chiral surface structures can also form for intrinsically achiral molecules if they are prochiral in the sense that chirality emerges due to reduced symmetry upon adsorption.[20,22,34,35] In this latter case, mirror-image surface enantiomers are always created in equal ratios for reasons of symmetry, and although these are often

Received: November 9, 2010
Published: March 14, 2011

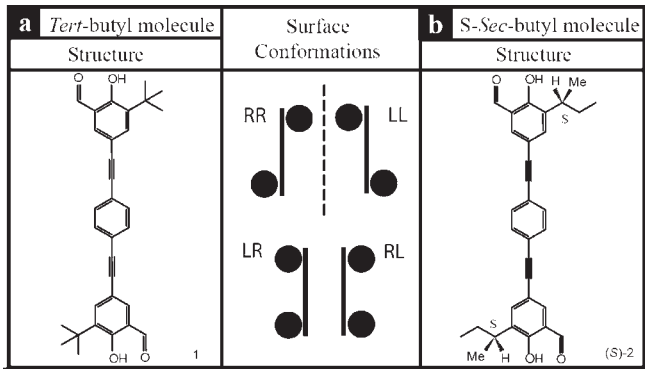

Figure 1. Rod-shaped molecules with oligo(phenylene ethynylene) (OPE) backbones and salicylaldehyde terminal groups. (a) Achiral *tert*-butyl-substituted variant **1** used in previous studies. (b) Intrinsically chiral (*S*)-*sec*-butyl-substituted variant (*S*)-**2** synthesized and used in the present investigation. The possible surface conformations are schematized in the central panel where the black circles represent the *tert*-butyl or (*S*)-*sec*-butyl groups, while the black rods represent the molecular backbone. The R and L (right and left) nomenclature refers to the position of the two *tert*/*sec*-butyl groups with respect to the molecular backbone when observing it from the central benzene ring. For **1**, the RR and LL conformations constitute mirror image surface enantiomers, while the RL/LR conformation is an achiral meso form. For (*S*)-**2**, the RR and LL conformations do not constitute surface enantiomers since the molecule is intrinsically chiral.

found to segregate into locally homochiral domains, the surface remains globally racemic.

We recently reported STM studies of the molecular rod **1**, which consists of an oligo(phenylene ethynylene) (OPE) backbone and two *tert*-butylsalicylaldehyde terminal groups (Figure 1a).[36−40] The achiral molecules **1** are prochiral and exhibit conformational chirality[40] in their adsorbed state since rotation of the end group around the axis of the ethynylene backbone allows different molecular conformations to be realized, two of which are mirror image enantiomers, which can be distinguished by the position of the *tert*-butyl groups with respect to the molecular backbone (Figure 1). When adsorbed on a Au(111) surface under ultrahigh vacuum (UHV) conditions, the molecules **1** form both a symmetric brick-wall structure as well as a network structure with a pronounced chiral organization of the molecular backbones in windmill motifs. In a subsequent study, we systematically modified the terminal group chemistry of **1** and demonstrated that it was thereby possible to steer the surface assemblies with respect to both conformational and organizational chirality.[40] However, since all the compounds synthesized for these studies were intrinsically achiral, the opposite conformational surface enantiomers and organizational windmill motifs, showing clockwise and counterclockwise sense of rotation, were necessarily always formed in equal proportion. This systematic investigation also demonstrated that even minor modifications to the molecular structure could lead to pronounced qualitative differences in the nature of the self-assembled structures formed, and most importantly, the windmill motifs only formed for those of the investigated compounds that retained both the hydroxyl and aldehyde moieties on their terminal groups.

In the present work, we focus on the challenge of using molecular design to achieve control over the absolute sense of the organizational chirality in assemblies formed from this class of compounds as manifested by the orientation of the molecular backbones in the windmill motifs. The presence of an asymmetric tetragonal carbon on an aliphatic side chain has previously been shown to influence the chirality of supramolecular surface assemblies, leading, for example, to enantiomeric separation[41] or a preferred arrangement of hydrogen-bonded chiral rosette motifs.[42,43] We therefore designed a molecule, (*S*)-**2**, in which the two *tert*-butyl groups in **1** are replaced with chiral (*S*)-*sec*-butyl groups (Figure 1b). This minimal modification of the overall structure results in a compound with the same empirical formula ($C_{32}H_{30}O_4$), an almost identical shape, and the hydrogen-bonding aldehyde/hydroxyl moieties retained. The enantiopure (e.e. > 99%) (*S*)-*sec*-butyl molecule (*S*)-**2** was synthesized from (*S*)-3-pheynylbutyric acid in 11 steps. The new molecule (*S*)-**2** was evaporated onto a Au(111) surface, and the self-assembled surface structures were characterized by high-resolution UHV-STM. We find that the perturbation to the molecular interactions by this subtle change in the molecular design is indeed sufficiently small that brickwall and windmill structures are formed with a very close similarity to those observed for **1**. In addition, we demonstrate by careful statistical analysis of STM images that the design of (*S*)-**2** creates a strong preference for one of the two possible rotation directions in the chiral windmill motifs formed by the molecular backbones and an associated preference for the RR over LL molecular conformation. These results constitute a significant demonstration of the state-of-the-art with respect to controlling chiral supramolecular surface assemblies by deliberate design of molecular building blocks.

RESULTS AND DISCUSSION

Chemical Synthesis. One of the key requirements for the synthesis of (*S*)-**2** has been to prepare the compound with a very high optical purity. Whereas the synthesis of compound **1** is straightforward,[39] the synthesis of (*S*)-**2** is a much greater challenge. An obvious key intermediate in the synthesis of the compound is the 3-(*S*)-*sec*-butyl-5-iodosalicylaldehyde, (*S*)-**9**, which after iodination and a Sonogashira cross-coupling with 1,4-bisethynylbenzene would lead to compound (*S*)-**2** (Scheme 1). Several unsuccessful attempts to prepare optically pure (*S*)-**9** were made such as chiral resolution of 2-*sec*-butylphenol,[44] enantioselective carbolithiation of allyl 2-bromophenyl ether followed by quenching with methyliodide leading to a cyclic ether that can be converted to 2-*sec*-butylphenol,[45] and asymmetric hydrogenation[46−49] of 1-(but-1-en-2-yl)-2-methoxybenzene.[50] However, only modest stereoselectively was observed for each of these methods. Finally, we devised a strategy based on (*S*)-3-phenylbutyric acid, (*S*)-**3**, which is commercially available (Scheme 1).

The synthesis was initiated by conversion of (*S*)-**3** into (*S*)-**4** in four steps following the strategy described Loiodice et al. (See Supporting Information for details).[51] The phenol (*S*)-**4** then was treated with benzoyl chloride under mild basic conditions to give the benzoyl-protected phenol (*S*)-**5** in 68% yield. Mild basic conditions were chosen to selectively protect the phenol and to avoid unwanted benzoylation of the primary alcohol. Treatment of (*S*)-**5** with iodine and triphenylphosphine converted the hydroxyl group to iodide (*S*)-**6** in 95% yield. The iodine moiety was removed by treatment with tributyltin hydride to give (*S*)-**7** in 89% yield. Finally, removal of the benzoyl protection group by treatment with potassium hydroxide did yield (*S*)-2-*sec*-butyl phenol ((*S*)-**8**). Skattebøl et al. have reported[52] that treatment of

Scheme 1

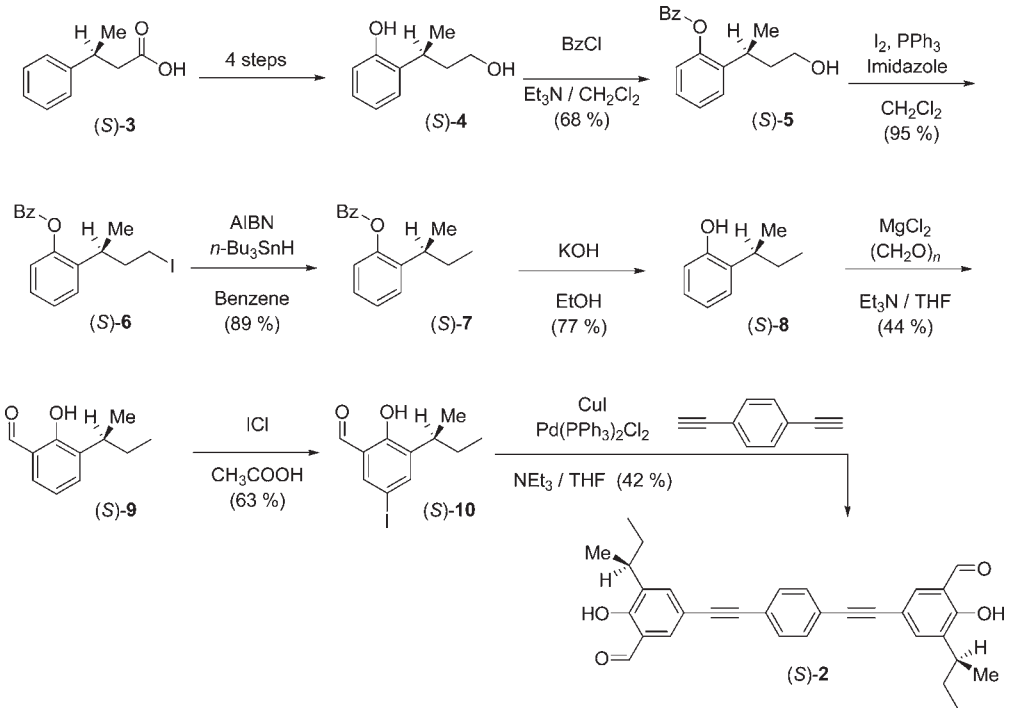

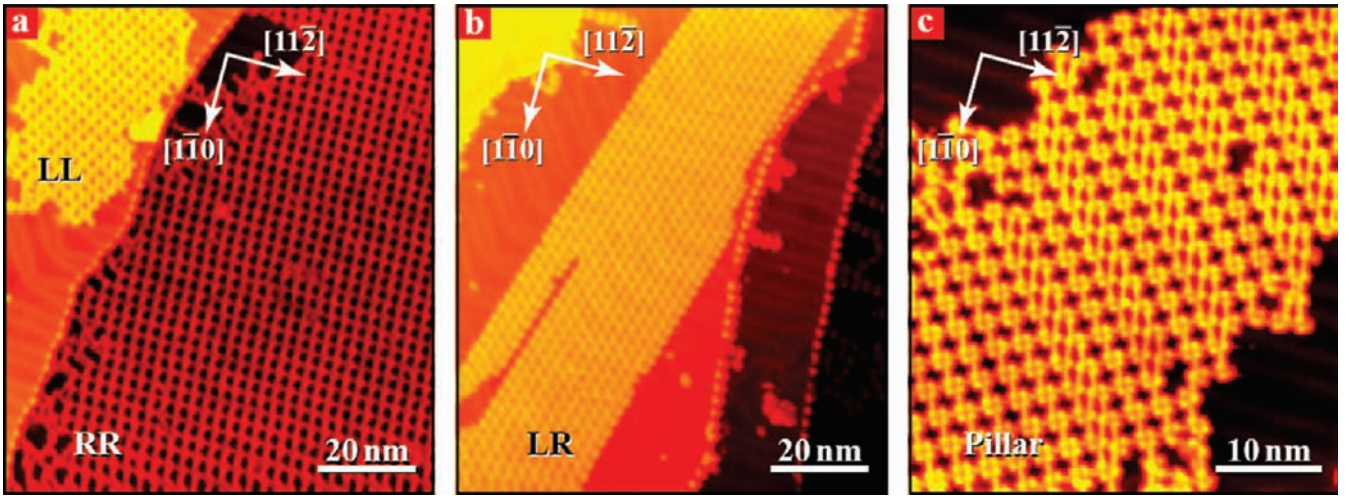

Figure 2. Large-scale STM images of molecular islands formed from (*S*)-**2** on the Au(111) surface: (a) RR and LL windmill structures; (b) LR brickwall structure; (c) pillar structure.

phenols with anhydrous manganese dichloride and paraformaldehyde leads to formylation with exclusive *ortho*-selectivity possibly due to coordination of the phenol moiety and formaldehyde to manganese to give the *ortho* product. We applied this protocol for (*S*)-**8** and isolated the formylated product ((*S*)-**9**) in a moderate yield of 44%. Alternative methods such as Duff or Reimer−Tiemann formylations were tested, but they lead to similar yields. Treatment of (*S*)-**9** with iodine monochloride, serving as an electrophilic iodine donor, lead to the iodinated product (*S*)-**10** in 63% yield. This compound was then reacted with *para*-diethynylbenzene under standard Sonogashira conditions resulting in the desired linear module (*S*)-**2** in 42% yield.

Growth and Characterization of Molecular Adsorption Structures. Following deposition of (*S*)-**2** on an atomically clean Au(111) surface (see Methods Section), well-ordered and compact monomolecular high islands were observed with a typical extension in the 50−100 nm range (see Figure 2). The STM imaging contrast in the interior of the islands was modulated by the characteristic pattern of the herringbone reconstruction, which we therefore conclude is preserved underneath the islands. The system displays structural polymorphism with several coexisting phases. Here we describe the two dominating windmill (Figure 2a) and brickwall (Figure 2b) phases. A number of additional minority structures (e.g., Figure 2c) are described in

dx.doi.org/10.1021/ja110052n |*J. Am. Chem. Soc.* 2011, 133, 4896–4905

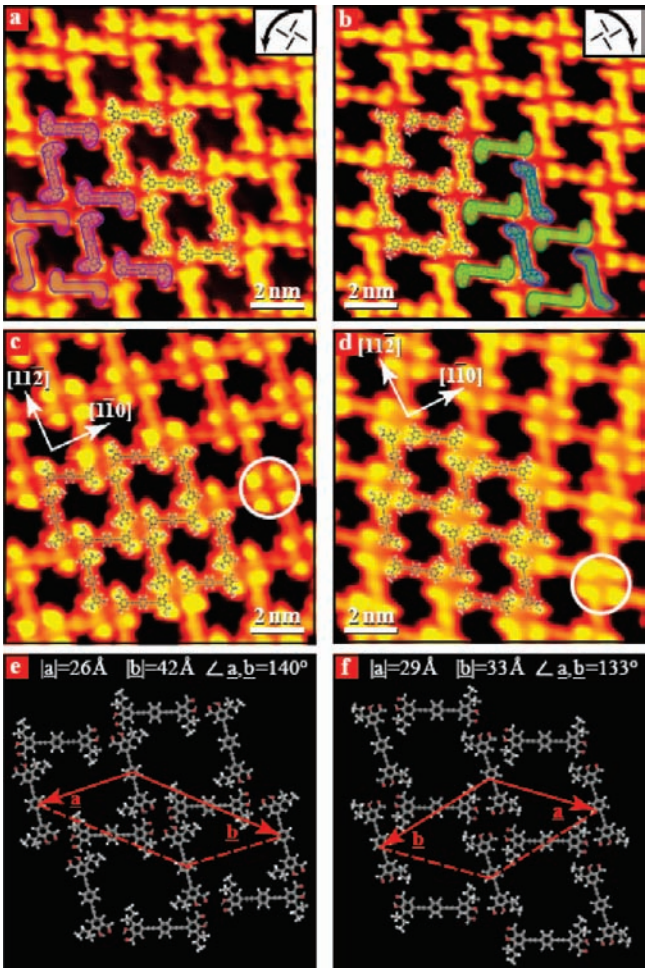

Figure 3. STM images and models of windmill structures formed from (*S*)-**2** on Au(111): (a) RR windmill structure with a counterclockwise rotation direction, observed in π-system imaging mode. Molecules are depicted in purple to underscore that the (*S*)-*sec*-butyl groups have the same geometry (120 × 120 Å^2, I_t = −0.5 nA, V_t = −1.28 V). (b) LL windmill structure with a clockwise rotation observed in π-system imaging mode. Molecules are depicted in green and blue to underscore that (*S*)-*sec*-butyl groups have two different geometries (120 × 120 Å^2, I_t = −0.5 nA, V_t = −1.24 V). (c) RR windmill structure observed in *sec*-butyl imaging mode (120 × 120 Å^2, I_t = −0.42 nA, V_t = −1.1 V). (d) LL windmill structure observed in *sec*-butyl imaging mode (120 × 120 Å^2, I_t = −0.45 nA, V_t = −1.04 V). (e) Proposed model of the RR windmill adsorption structure as deduced from the STM image. (f) Proposed model of the LL windmill adsorption structure as deduced from the STM image.

the Supporting Information. The molecular structures were observed in two distinct STM imaging modes. In the "π-system imaging mode", the conjugated OPE molecular backbone is the most prominent feature and its three benzene rings can typically be resolved. In the "*sec*-butyl imaging mode", dominating protrusions are seen to the sides of the molecular backbones, which are attributed to the (*S*)-*sec*-butyl groups. Similar imaging modes were observed for the related *tert*-butyl-substituted OPE compounds[36,38,40] and are ascribed to different STM tip apex terminations, which could not be controlled at will. The two imaging modes are complementary and conveniently allow assignment of both (i) the organizational pattern of the molecular backbones and (ii) the molecular conformation in regard to the position (L/R) of the *sec*-butyl group with respect to the molecular backbone.

RR and LL Windmill Phases. Figure 3 shows high-resolution STM images and associated models of the windmill structure. The STM image displayed in Figure 3a is obtained in the π-system imaging mode and shows the OPE molecular backbones of (*S*)-**2** adsorbed parallel to the surface plane and arranged in characteristic windmill motifs formed from four molecular backbones joined in a common node. Each molecular backbone connects two such nodes forming an extended network with rhombic openings surrounded by four molecules. Figure 3c shows the same structure observed in the *sec*-butyl imaging mode. Here, four bright protrusions, each attributed to a (*S*)-*sec*-butyl group, are clearly distinguishable at every node (e.g., see the node marked by a white circle in Figure 3c). In all cases, the *sec*-butyl protrusions are positioned to the right of the molecular backbones (when viewed from the center of the molecules), and all the molecules in the structure are thus adsorbed in the RR conformation. A related windmill structure with an opposite clockwise arrangement of the windmill motifs is also observed on the surface, as shown in Figure 3b (see insets in Figure 3a,b for definition of counterclockwise/clockwise rotation direction). In this situation, all the molecules assume the LL conformation as seen from the STM image of Figure 3d, obtained in the *sec*-butyl imaging mode. The position of the *sec*-butyl groups at the outside of the windmill nodes implies that the hydroxyl and aldehyde terminal functionalities of the four joined molecules point toward the node interior and hydrogen-bonding interactions between these moieties most likely contribute to the cohesion of the windmill networks as discussed in detail for related compounds.[40]

The two described windmill structures show perfect correlation between the organizational pattern of the molecular backbones and the surface conformation of the adsorbed molecules; the RR-windmill structure with a counterclockwise rotating windmill motif is composed exclusively of RR conformers (Figure 3a,c), while the LL-windmill structure with a clockwise rotating windmill motif is composed of LL conformers (Figure 3 b,d). An entirely similar organizational behavior was observed for the *tert*-butyl molecules **1**.[38,40] However, while the RR and LL windmill structures of **1** are mirror image domains formed from opposite conformational surface enantiomers, the two windmill structures formed by (*S*)-**2** cannot be exact mirror images of each other since the (*S*)-*sec*-butyl-substituted molecules are intrinsically chiral. The two structures must therefore be considered distinct surface phases. Careful determination of unit cell parameters for the RR and LL windmill phases, as reported in the structural models of Figure 3e,f, in fact, also show a small but significant deviation between them.

A number of related minority structures are described in the Supporting Information. In brief, two structures ("cross" and "complex") have windmill arrangements that deviate slightly from the one described above but show the same correlation between molecular conformation and windmill sense of rotation (Figure S1, Supporting Information). The "pillar" structure occurs where stacking faults between windmill domains of the same handedness are connected by rows (pillars) of molecules (Figure 2c and Figure S2, Supporting Information). The connecting molecules assume the opposite conformation compared with those in the surrounding windmill domains, that is, RR pillars connecting LL windmills and *vice versa*.

RL Brick-Wall Phase. Figure 4 shows high-resolution STM images and an associated model of the brick-wall structure. STM images obtained in the π-system imaging mode (Figure 4a)

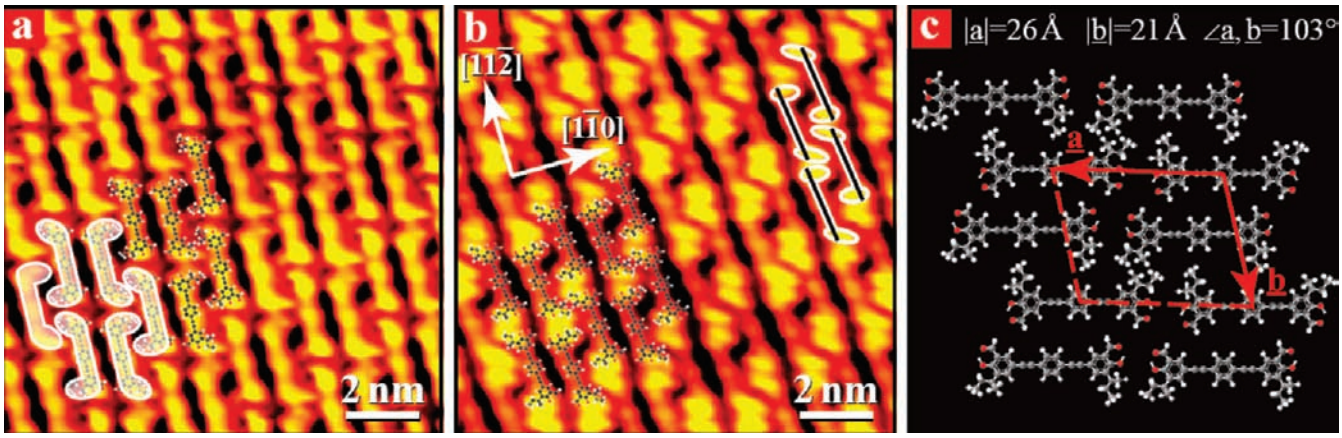

Figure 4. The brick-wall structure formed by (*S*)-**2** on Au(111). (a) STM image obtained in the π-system imaging mode with molecular models superimposed (120×120 Å^2, $I_t = -0.45$ nA, $V_t = -1.28$ V). (b) STM image obtained in the *sec*-butyl imaging mode (120×120 Å^2, $I_t = -0.45$ nA, $V_t = -1.04$ V). The schematic models indicate the two different (*S*)-*sec*-butyl group geometries as discussed in the text. (c) Proposed model of the brick-wall adsorption structure as deduced from the STM image.

reveal that the (*S*)-**2** molecules self-assemble in a regular tiling pattern in which the molecular backbones stack end to end forming extended rows that align parallel to each other. Each molecular backbone is slightly rotated compared with the row direction. As seen from Figure 4b, the two *sec*-butyl protrusions on a given molecule are both located at the same side of the backbone, that is, all molecules in the brickwall structure are in RL conformation. The structure can be rationalized as composed of double rows formed by pairing two adjacent rows for which all the (*S*)-*sec*-butyl groups point toward the interior of the pair. The backbones in the two rows composing a double row are shifted along the row direction by approximately half the repeat distance along the rows while the shift between adjacent double rows is smaller. Within the double rows, the (*S*)-*sec*-butyl groups in L conformation lie very close to each other, while the (*S*)-*sec*-butyl groups in R conformation are spaced further apart and point toward the central portion of the backbone belonging to a neighboring molecule from the adjacent row (see Figure 4c and the molecular models superimposed on the STM images).

The brickwall structure described here should be compared with the corresponding brickwall structure formed from the *tert*-butyl-substituted compound **1**.[38,40] The two structures are quite similar with respect to the row-like stacking of the molecular backbones, although the brickwall structure of **1** has higher symmetry with identical shifts between adjacent rows, thereby avoiding the pairing of rows observed here. The most noticeable difference is in the molecular conformations assumed within the structures. Whereas the present structure is well-ordered and consists exclusively of molecules in RL conformation, the brick-wall structure of **1** is conformationally disordered and encompasses all three possible surface conformations (i.e., RR, LL, and RL/LR). The ordered arrangement of RL conformers observed here implies that the *sec*-butyl groups on neighboring molecules are always positioned to the same side of the molecular rows when molecules meet end-to-end along the rows (*cis*-arrangement). This is in contrast to the brickwall structure of **1** where an arrangement placing the bulky groups on opposite sides of the rows was statistically preferred (*trans*-arrangement). By contrast, a preference for *cis*-arrangement of neighboring *tert*-butyl groups was also observed for derivatives of **1** where the aldehyde or hydroxyl groups were either removed or chemically modified to prevent intermolecular hydrogen bonding,[40] and one of these compounds was observed to form an ordered brickwall structure very similar to the one observed here for (*S*)-**2**. We therefore suggest that the order in the brickwall structure of (*S*)-**2** arises primarily from interactions between the *sec*-butyl groups. This occurs partly where neighboring groups meet along the rows in *cis*-arrangement, but in particular within the double rows where the *sec*-butyl groups in L conformation lie in very close proximity, possibly interlocking the two rows of molecules belonging to a double row (see Figure 4c). A similar interlocking of even larger aliphatic side groups was observed for a related compound in a different study.[53,54]

Statistical Analysis. The (*S*)-*sec*-butyl-substituted compound (*S*)-**2** thus forms windmill and brickwall phases that are structurally similar to those formed by the initially studied *tert*-butyl-substituted compound **1**,[38] demonstrating that the modified molecular design indeed only implies a minor perturbation to the intermolecular and molecule−substrate interactions. The prochiral *tert*-butyl molecules **1** by symmetry form the two enantiopure windmill domains with equal probability for the two opposite chiralities exhibiting LL/RR molecular conformation and clockwise/counterclockwise rotating windmill motifs, respectively. However, for (*S*)-**2** a preference for one of the two opposite windmill arrangements is anticipated due to the asymmetry introduced by the chiral centers of the (*S*)-*sec*-butyl moieties.

To address this question with a local probe technique such as STM, a careful statistical sampling of the structures occurring on the surface is required. The scanner head of our STM allows an area of nominally 2 μm $\times$ 2 μm of the Au(111) surface to be covered without physically moving the sample. We systematically surveyed 31 such sample areas obtained from a total of 8 preparations of molecular adsorption structures using identical experimental conditions. The survey was performed using image sizes of typically $\sim 100 \times 100$ nm^2, to allow covering large enough areas to ensure an efficient sampling and minimizing the risk of missing or double-counting molecular islands. Each $\sim 100 \times 100$ nm^2 image was acquired after shifting the tip position by at least 70−100 nm in *x* or *y* direction from the previous sampling position. By this procedure, we typically observed ~20 individual islands per 2 μm $\times$ 2 μm sample area. The molecular structure

dx.doi.org/10.1021/ja110052n |*J. Am. Chem. Soc.* 2011, 133, 4896–4905

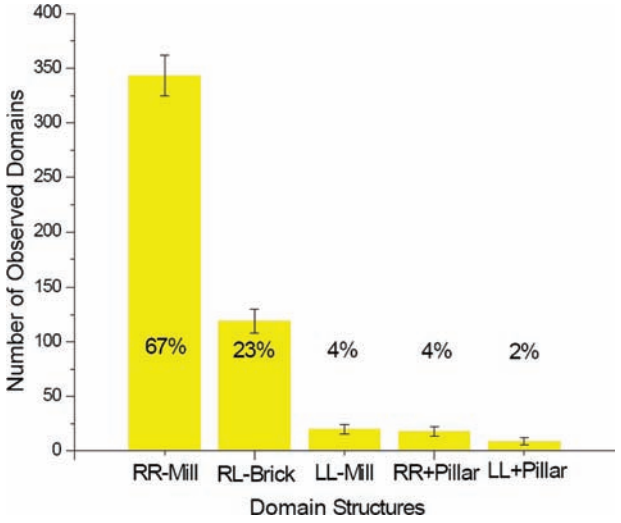

Figure 5. Histogram showing the number of observations of domains with different adsorption structure as defined in the text. The relative occurrences are indicated as percentages.

within the islands was identified from high-resolution ~30 × 30 nm^2 images.

The observed domains were categorized as follows: (i) windmill domains of either RR or LL kind (the closely related "complex" and "cross" phases described in the Supporting Information were included in this category but constituted only a minor proportion of the observations), (ii) RL brickwall domains, and (iii) pillar domains involving either RR or LL windmills. These latter domains were registered separately since they involve a mixing of RR and LL conformers (see the Supporting Information.). The islands typically consisted of a single structural domain, but in cases where two or more domains coexisted within one island, these were counted separately. A total of 509 domains were observed from the statistical analysis. A histogram showing the distribution of domain types is displayed in Figure 5. The pillar structures constitute only a very small proportion of the observed domains. The next category is RL brickwall domains, which constituted 23%. By far the most frequent pattern of (*S*)-**2** was the windmill structure. Here there is a striking asymmetry between the RR and LL windmill structures, which were observed for 67% and 4% of the domains, respectively. Very importantly the (*S*)-*sec*-butyl-substituted compound thus indeed shows a very strong preference for one of the two windmill tiling patterns for the molecular backbones.

The domain-based analysis should be combined with information on the relative island sizes. The RR windmill islands typically extend well beyond the borders of the 100 × 100 nm^2 images, while the LL islands have a considerably smaller area, we judge by a factor of ~10. The domain-based analysis therefore provides a very conservative estimate of the ratio between the number of molecules in RR and LL conformations. The RL brickwall islands are elongated along the direction of the molecular backbones, and in this direction they typically extend beyond the boundaries of the STM images. However, we judge that these islands typically do not cover a larger area than the RR islands. A full molecular-level analysis, determining the fraction of molecules adsorbed in each of the different domain types rather than the number of observed domains, is complicated by domains that exceed the boundaries of the STM images and requires either a complex analysis to avoid, for example, double counting resulting from overlapping images showing the same portion of the surface or a completely random sampling of the surface.

While a clear preference for structures with the counterclockwise RR windmill motif is observed, a portion of the surface is still covered by molecules in brickwall structure. We previously showed that it is possible by molecular design to steer the surface assembly of the linear OPE compounds so that the brickwall structure is avoided and only the windmill structure is formed, but in this case with the two chiral domains occurring in equal proportion since a prochiral compound was used.[40] It is however unclear how the two design strategies might be combined, since the OPE prochiral compound forming exclusively windmill structures was precisely the one synthesized without a *tert*-butyl substituent on the terminal group and it is therefore not possible in this case to exchange the *tert*-butyl group by a chiral *sec*-butyl group.

(*S*)-*sec*-Butyl Group Conformation. As demonstrated from the statistical analysis, it is indeed possible by molecular design to induce a preference for one of the chiral tiling patterns of the OPE molecular backbones. To discuss the dynamic and energetic origin of this preference, we first note that we previously demonstrated for the *tert*-butyl molecule **1** and related compounds that the terminal groups can undergo a thermally activated half-turn rotation around the molecular axis even after adsorption on the Au(111) surface, thereby allowing the molecules to switch between the R and L conformations.[36,38,40] The conformational switching allows the molecule to accommodate to the preferred conformation/chirality assumed in a given pattern. We therefore assume that the terminal group of (*S*)-**2** can undergo a similar switching on the surface allowing it to probe both the R and L conformations. For **1**, the minimum adsorption energies in the R and L situations are identical because of the symmetry of the *tert*-butyl substituent. However, due to the chiral nature of the (*S*)-*sec*-butyl group in (*S*)-**2** we expect a small energy difference between the two surface conformations of the terminal groups, making growth of structures involving the lower-energy conformation favored. This is indeed what is observed in the experiments where a clear preference for the windmill structure based on the RR conformer of (*S*)-**2** is observed.

To explicitly see how the chirality of the (*S*)-*sec*-butyl group may introduce an energy difference between the R and L conformations of the terminal group, we show in Figure 6 Newman projections and schematic side views of possible adsorption geometries for the (*S*)-*sec*-butyl group. In the leftmost panel of Figure 6, a situation is depicted where the terminal group is in R conformation, denoted (*S*)-R. If the terminal group is rotated to the L conformation, as shown in the right panel of Figure 6, it is not possible by rotations or conformational changes of the (*S*)-*sec*-butyl group to realize a situation where it is adsorbed in an identical arrangement. This is due to the chiral center and fundamentally explains why an energy difference is to be expected between the R and L conformations of the *sec*-butyl-substituted compound (*S*)-**2**. Further insight into why an R conformation is energetically preferred over L may be obtained by analysis of the possible local conformations of the (*S*)-*sec*-butyl group when absorbed on the surface. For the (*S*)-R situation, a conformation is chosen for the (*S*)-*sec*-butyl group where the H atom points toward the surface, the steric hindrance between the ethyl chain and the hydroxyl group is minimized,

dx.doi.org/10.1021/ja110052n |*J. Am. Chem. Soc.* 2011, 133, 4896–4905

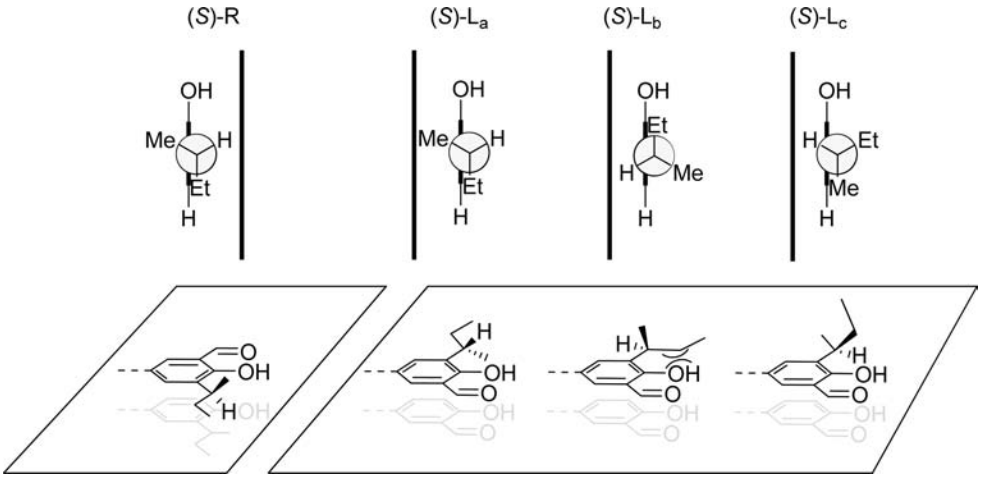

Figure 6. Possible surface adsorption geometries for (*S*)-*sec*-butyl-substituted terminal groups in R and L conformation. One model is reported for the R conformation, (*S*)-R, while three different models are reported for L, (*S*)-L_a, (*S*)-L_b, and (*S*)-L_c. Upper panel, Newman projections with the surface schematized by the thick line. Lower panel, corresponding side-view representations of the same terminal group conformations on the surface. The connection to the molecular backbone is indicated by the dashed line.

and the ethyl chain is adsorbed parallel to the surface, which is generally observed to be preferred for alkyl chains. In the (*S*)-L case, we restrict the discussion to three conformations: The first, (*S*)-L_a, results from direct rotation of the shown (*S*)-R conformation with the consequence that the methyl group is pointing toward the surface, which is expected to be unfavorable due to steric repulsion. In the second conformation, (*S*)-L_b, the H is pointing toward the surface, but this conformation may give rise to steric repulsion between the ethyl chain and the hydroxyl group. In the third conformation, (*S*)-L_c, the H is again pointing toward the surface. The last model would minimize steric hindrance compared with the other two L conformations, however, at the price of less stabilizing adsorption geometry with the ethyl group pointing away from the surface. Other conformations for (*S*)-L are possible, however, in general we find that a preference for (*S*)-R is to be expected, since it minimizes steric hindrance while optimizing the interaction with the surface.

This analysis suggests there should be differences in the adsorption orientation for the *sec*-butyl group when the terminal group of (*S*)-**2** assumes L and R conformations. The high-resolution STM images indeed present support for this notion in terms of subtle differences in the appearance of the *sec*-butyl protrusions in dependence on their orientation (R/L) with respect to the molecular backbone. This is seen most clearly for the brickwall structure where the individual molecules realize both conformations. Careful scrutiny of Figure 4b reveals that the *sec*-butyl-related protrusions in R orientation point nearly perpendicular to the molecular backbone, while the protrusions in L orientation are rotated by a larger angle (the difference is indicated by white ellipsoidal overlays in Figure 4b). In the adsorption model of Figure 4c, the two (*S*)-*sec*-butyl groups on a given molecule are both drawn in conformations with the H pointing toward the surface. As a consequence, the group in (*S*)-R conformation has the ethyl chain perpendicular to the molecular backbone, while the other group, in position (*S*)-L, has to rotate to point the H atom toward the surface, thus positioning the ethyl chain more parallel to the molecular backbone, as for the conformation (*S*)-L_b discussed above. These orientations for the ethyl chain agree well with the appearance of the *sec*-butyl protrusions in the STM image.

For the LL windmill structure, where the *sec*-butyl groups are forced to assume the unfavorable LL conformation, it is possible to distinguish a subtle difference in the appearance of the *sec*-butyl protrusions on molecules in different orientations as indicated by blue and green overlays in Figure 3b. In the structural model of Figure 3f, the two molecules in the LL windmill indicated by green color are therefore drawn in conformation (*S*)-L_a (i.e., pointing the (*S*)-*sec*-butyl group methyl toward the surface), while the other two (blue) are drawn in conformation (*S*)-L_b (i.e., pointing the (*S*)-*sec*-butyl group H toward the surface). For the RR windmill structure, there appears to be no systematic difference between the appearances of the *sec*-butyl protrusions in the STM images of Figure 3a,c. Therefore the (*S*)-*sec*-butyl groups are all assumed to be in the (*S*)-R conformation in the model drawn in Figure 3e (this is also the case for the cross and complex windmill patterns, see Supporting Information).

CONCLUSIONS

We have designed and synthesized a novel building block for molecular surface self-assembly with interactions that are fine-tuned to allow exquisite control over the chirality of the formed adsorption structures. The design is based on a previously studied rod-shaped molecule and involves the replacement of two achiral *tert*-butyl side groups with chiral (*S*)-*sec*-butyl moieties, rendering the originally prochiral molecule intrinsically chiral. The perturbation introduced by the modified molecular design is demonstrated to be sufficiently small that the new compound upon adsorption on the Au(111) surface forms windmill and brickwall structures that are closely analogous to those observed for the original *tert*-butyl compound. However, as shown by careful statistical analysis of STM images, the introduction of the two chiral (*S*)-*sec*-butyl substituents leads to a strong preference for adsorption in the RR molecular surface conformation and for formation of windmill motifs with one sense of rotation, demonstrating that the chiral organization of the molecular backbones can be controlled by molecular design. The origin of this chiral preference is rationalized from qualitative

adsorption models for situations where the (*S*)-*sec*-butyl-substituted molecules assume R and L surface conformations. Further studies will address whether the novel enantiopure (*S*)-*sec*-butyl compound can be used in coadsorption experiments as a seed to induce[55] a chiral preference in the windmill adsorption structures formed from the original prochiral *tert*-butyl compound.

METHODS SECTION

Molecular Deposition and UHV-STM Experiments. Growth and characterization of molecular adsorption structures was performed in an ultrahigh vacuum system with a base pressure in the low 10^{-10} mbar regime and equipped with a home-built variable-temperature Aarhus STM.[56] The Au(111) single crystal was cleaned by several cycles of 1.5 keV Ar^+ sputtering followed by annealing at 850 K, resulting in an atomically clean (22 × $\sqrt{3}$) herringbone reconstructed Au(111) surface. The enantiopure *sec*-butyl molecules (*S*)-**2** were sublimated from a resistively heated glass crucible maintained at 378 K and held within a few centimeters from the Au surface. Typical dosing times were 1−1.5 min resulting in a molecular surface coverage in the range of 55−75% of a saturated first monolayer. The Au(111) substrate was held at room temperature (∼300 K) during molecular deposition and was subsequently cooled gradually (6 K/min) to 125 K to allow formation of ordered molecular surface structures. STM images were acquired in the temperature range 120−130 K.

Synthesis of (*S*)-4. The synthesis of (*S*)-**4** from commercially available (*S*)-**3** is described in the Supporting Information.[51]

(*S*)-Benzoic acid 2-(3-hydroxy-1-methyl-propyl)-phenyl ester ((*S*)-5). To a stirred solution of (*S*)-**4** (1.40 g, 8.42 mmol) and triethylamine (2 mL) in CH_2Cl_2 (20 mL) was slowly added benzoyl chloride (0.98 mL, 8.42 mmol), and the mixture was stirred for 2 h at room temperature. The reaction mixture was extracted with saturated NH_4Cl and water and dried ($MgSO_4$), and the solvent was removed *in vacuo*. The residue was purified by flash chromatography (CH_2Cl_2) to yield 1.55 g (68%) of the desired product as a colorless oil. ^{1}H NMR (400 MHz, $CDCl_3$) δ 8.22 (d, J = 8.0 Hz, 2H), 7.65 (t, J = 7.6 Hz; 1H), 7.53 (t, J = 7.2 Hz, 2H), 7.34−7.26 (m, 3H), 7.14−7.11 (m, 1H), 3.54 (m, 2H), 3.12 (m, 1H), 1.86 (q, J = 6.8 Hz, 2H), 1.25 (d, J = 7.2 Hz, 3H). ^{13}C NMR (100 MHz, $CDCl_3$) δ 134.0; 130.4; 130.4; 128.9; 128.9; 127.6; 127.3; 126.8; 122.7; 61.0; 40.2; 29.3; 22.3. HRMS (ES) m/z: [M + Na] calcd for $C_{17}H_{18}NaO_3$ 293.1154; found 293.1142.

(*S*)-Benzoic acid 2-(3-iodo-1-methyl-propyl)-phenyl ester ((*S*)-6). To a solution of (*S*)-**5** (660 mg, 2.41 mmol) in a mixture of THF (10 mL) and CH_3CN (20 mL) was sequentially added imidazole (650 mg, 9.9 mmol), triphenylphosphine (3.2 g, 12.2 mmol), and iodine (3.1 g, 12.2 mmol), and the mixture was stirred for 45 min at room temperature when TLC analysis revealed full consumption of starting material. The mixture was poured into 50 mL of EtOAc and extracted twice with an aqueous solution of $Na_2S_2O_3$, then with brine and H_2O, and dried over $MgSO_4$. The solvent was removed *in vacuo*, and the residue was purified by flash chromatography (hexanes/CH_2Cl_2 2:1, R_f = 0.25) to yield 870 mg (95%) of the desired product as a colorless oil. ^{1}H NMR (400 MHz, $CDCl_3$) δ 8.25 (d, J = 8.0 Hz, 2H), 7.66 (t, J = 7.2 Hz; 1H), 7.54 (t, J = 7.6 Hz, 2H), 7.34−7.27 (m, 3H), 7.14−7.11 (m, 1H), 3.17−2.97 (m, 3H), 2.25−1.97 (m, 2H), 1.25 (d, J = 7.2 Hz, 3H), ^{13}C NMR (100 MHz, $CDCl_3$) δ 165.5; 148.9; 137.4; 133.9; 130.5; 129.5; 128.8; 127.6; 127.5; 126.8; 123.0; 41.3; 34.0; 21.0; 4.7. HRMS (ES) m/z: [M + Na] calcd for $C_{17}H_{17}INaO_2$ 403.0171; found 403.0189.

(*S*)-Benzoic acid 2-*sec*-butyl-phenyl ester ((*S*)-7). A solution of (*S*)-**6** (830 mg, 2.2 mmol) and AIBN (66 mg, 0.40 mmol) in benzene (5 mL) was stirred for 30 min. *n*-Bu_3SnH (1.2 mL, 4.4 mmol) was slowly added, and the solution was heated to 70 °C for 3 h then allowed to cool to room temperature. The mixture was extracted with H_2O and dried ($MgSO_4$), and the solvent was removed *in vacuo*. The residue was purified by flash chromatography (CH_2Cl_2/hexanes 1:1) to yield 498 mg (89%) of the desired product as a colorless oil. ^{1}H NMR (400 MHz, $CDCl_3$) δ 8.24 (d, J = 8.0 Hz, 2H), 7.68 (t, J = 7.2 Hz; 1H), 7.54 (t, J = 7.6 Hz, 2H), 7.34−7.25 (m, 3H), 7.14−7.11 (m, 1H), 2.87 (m, 1H), 1.42−1.34 (m, 2H), 1.22 (d, J = 7.2 Hz, 3H), 0.82 (t, J = 7.6 Hz, 3H), ^{13}C NMR (100 MHz, $CDCl_3$) δ 165.4; 148.9; 139.4; 133.8; 130.3; 129.8; 128.8; 127.5; 126.8; 126.5; 122.6; 34.7; 30.5; 21.1; 12.4. HRMS (ES) m/z: [M + Na] calcd for $C_{17}H_{18}NaO_2$ 277.1204; found 277.1219.

(*S*)-2-*sec*-Butyl-phenol ((*S*)-8). Compound (*S*)-**7** (400 mg, 1.6 mmol) was dissolved in EtOH (10 mL), and 10 M aqueous NaOH (1 mL, 10 mmol) was added. The reaction mixture was heated to reflux and stirred for 3 h. The mixture was cooled to room temperature and then made neutral by addition of 1 M aq. HCl. Extraction with CH_2Cl_2, drying ($MgSO_4$), removal of the solvent, and purification by column chromatography yielded 185 mg (77%) of the product, which is identical to commercially available racemic 2-*sec*-butylphenol.

(*S*)-3-*sec*-Butyl-2-hydroxy-benzaldehyde ((*S*)-9). To a stirred suspension of (*S*)-**8** (250 mg, 1.67 mmol), anhydrous magnesium chloride (320 mg, 3.33 mmol), and dry paraformaldehyde (100 mg, 3.33 mmol) in dry THF (15 mL), triethylamine (0.5 mL) was added dropwise. The reaction mixture was refluxed for 2 h and allowed to cool to room temperature. The reaction mixture was poured into saturated aqueous NH_4Cl and extracted several times with CH_2Cl_2. The organic phase was dried ($MgSO_4$), and the solvent was removed *in vacuo*. The residue was purified by column chromatography (hexanes/CH_2Cl_2 1:1, R_f = 0.5) to yield 130 mg (44%) of the desired product as a yellow oil. ^{1}H NMR (400 MHz, $CDCl_3$) δ 11.27 (s, 1H), 9.79 (s, 1H), 7.34 (d, J = 7.6 Hz, 1H), 7.30 (d, J = 7.6 Hz, 1H), 6.90 (t, J 7.6 Hz, 1H), 3.08 (m 1H), 1.52 (m, 2H), 1.14 (d, J = 7.6 Hz, 3H), 0.77 (t, J = 7.2 Hz, 3H). ^{13}C NMR (100 MHz, $CDCl_3$) δ 197.2; 159.7; 136.2; 134.7; 131.6; 120.4; 119.8; 33.1; 29.7; 20.3; 12.2. HRMS (ES) m/z: [M + Na] calcd for $C_{11}H_{14}NaO_2$ 201.0891; found 201.0894.

(*S*)-3-*sec*-Butyl-2-hydroxy-5-iodo-benzaldehyde ((*S*)-10). Compound (*S*)-**9** (75 mg, 0.56 mmol) was dissolved in glacial acetic acid (5 mL) in a 25 mL round-bottomed flask equipped with a reflux condenser. Iodine monochloride (133 mg, 0.82 mmol) suspended in glacial acetic acid (2 mL) was added dropwise to the solution, and the reaction mixture was refluxed for 4 h. The mixture was allowed to cool to room temperature and poured into water (30 mL), and 20 mL of aqueous sodium thiosulfate was added. The solution was extracted several times with CH_2Cl_2, the organic phase was dried ($MgSO_4$), and the solvent was removed *in vacuo*. The residue was purified by column chromatography (silica gel, 10% ether in pentane, R_f = 0.3) to yield 107 mg (63%) of the desired product as a yellow oil after removal of the solvent. ^{1}H NMR (400 MHz, $CDCl_3$) δ 11.21 (s, 1H), 9.74 (s, 1H), 7.62 (d, J = 2 Hz, 1H), 7.57 (d, J = 2 Hz, 1H), 3.02 (m, 1H), 1.53 (m, 2H), 1.14 (d, J = 7.2 Hz, 3H), 0.79 (t, J = 7.2 Hz, 3 H). ^{13}C NMR (100 MHz, $CDCl_3$) δ 196.2; 164.2; 161.0; 142.6; 141.6; 140.2; 122.5; 33.6; 29.7; 20.3; 12.2. HRMS (ES) m/z: [M + Na] calcd for $C_{11}H_{13}INaO_2$ 326.9858; found 326.9861.

(*S,S*)-1,4-Bis((5-*sec*-butyl-4-hydroxy-3-formylphenyl)-ethynyl)benzene ((*S*)-2). A mixture of (*S*)-**10** (70 mg, 0.23 mmol), CuI (4 mg, 0.02 mmol), and $Pd(PPh_3)_2Cl_2$ (16 mg, 0.02 mmol) were stirred in for 1 h under vacuum in a flame-dried Schlenk flask. A degassed solution of 1,4-diethynylbenzene (15 mg, 0.13 mmol) in triethylamine (0.7 mL) and THF (5 mL) was added, and the mixture was stirred for 12 h at 50 °C under an argon atmosphere. The reaction mixture was allowed to cool to room temperature and filtered through a pad of Celite, and the residue was partitioned between CH_2Cl_2 (15 mL) and aqueous ammonium chloride (10 mL). The organic layer was separated, and the aqueous phase was extracted twice with CH_2Cl_2 (10 mL). The combined organic phase was dried ($MgSO_4$), and the solvent was

removed *in vacuo*. The residue was purified by column chromatography (CH_2Cl_2, $R_f = 0.3$) to yield 46 mg (42%) of the product as a yellow solid after removal of the solvent. ^{1}H NMR (400 MHz, $CDCl_3$) δ 11.50 (s, 2H), 9.99 (s, 2H), 7.61 (d, $J = 2.0$ Hz, 2H), 7.57 (d, $J = 2.0$ Hz, 2H), 7.51 (s, 4H), 3.16 (q, $J = 7.2$ Hz, 2H), 1.65 (dq, $J = 13.6, 7.6$ Hz, 4H), 1.24 (d, $J = 6.8$ Hz, 6H), 0.88 (t, $J = 6.8$ Hz, 6H). ^{13}C NMR (100 MHz, $CDCl_3$) δ 196.6 (2C); 159.9 (2C); 137.5 (2C); 137.1 (2C); 134.9 (2C); 131.7 (4C); 123.1 (2C); 120.3 (2C); 114.6 (2C); 90.4 (2C); 88.4 (2C); 33.2 (2C); 29.6 (2C); 20.3 (2C); 12.3 (2C). MS (MALDI TOF) *m/z*: MH calcd for $C_{32}H_{30}O_4$ 478.2; found 478.1.

Racemic **2** linear module was synthesized starting from racemic 2-*sec*-butylphenol **8** in a similar way as the chiral compound.

■ ASSOCIATED CONTENT

Supporting Information. Descriptions and UHV-STM images of minority absorption structures, general methods, synthesis of (*S*)-**4**, ^{1}H and ^{13}C NMR spectra. This material is available free of charge via the Internet at http://pubs.acs.org.

■ AUTHOR INFORMATION

Corresponding Author

*E-mail addresses: trolle@inano.au.dk, kvg@chem.au.dk.

■ ACKNOWLEDGMENT

We acknowledge financial support from the Marie-Curie EST MONET and ITN SMALL, The Danish Council for Independent Research | Natural Sciences, The Villum Foundation, and the Danish National Research Foundation for support to CDNA and the Sino-Danish Center for Molecular Nanostructures on Surfaces.

■ REFERENCES

(1) Barth, J. V. *Annu. Rev. Phys. Chem.* **2007**, *58*, 375–407.
(2) Elemans, J.; Lei, S. B.; De Feyter, S. *Angew. Chem., Int. Ed.* **2009**, *48*, 7298–7332.
(3) Tomba, G.; Ciacchi, L. C.; De Vita, A. *Adv. Mater.* **2009**, *21*, 1055–1066.
(4) Liang, H.; He, Y.; Ye, Y. C.; Xu, X. G.; Cheng, F.; Sun, W.; Shao, X.; Wang, Y. F.; Li, J. L.; Wu, K. *Coord. Chem. Rev.* **2009**, *253*, 2959–2979.
(5) Bonifazi, D.; Mohnani, S.; Llanes-Pallas, A. *Chem.—Eur. J.* **2009**, *15*, 7004–7025.
(6) Ciesielski, A.; Palma, C. A.; Bonini, M.; Samori, P. *Adv. Mater.* **2010**, *22*, 3506–3520.
(7) Cicoira, F.; Santato, C.; Rosei, F. In *STM and AFM Studies on (Bio)molecular Systems: Unravelling the Nanoworld*; Samorí, P., Ed.; Springer: Berlin, 2008; Vol. 285, pp 203−267.
(8) Yokoyama, T.; Yokoyama, S.; Kamikado, T.; Okuno, Y.; Mashiko, S. *Nature* **2001**, *413*, 619–621.
(9) Schlickum, U.; Decker, R.; Klappenberger, F.; Zoppellaro, G.; Klyatskaya, S.; Ruben, M.; Silanes, I.; Arnau, A.; Kern, K.; Brune, H.; Barth, J. V. *Nano Lett.* **2007**, *7*, 3813–3817.
(10) Tahara, K.; Furukawa, S.; Uji-I, H.; Uchino, T.; Ichikawa, T.; Zhang, J.; Mamdouh, W.; Sonoda, M.; De Schryver, F. C.; De Feyter, S.; Tobe, Y. *J. Am. Chem. Soc.* **2006**, *128*, 16613–16625.
(11) Wintjes, N.; Hornung, J.; Lobo-Checa, J.; Voigt, T.; Samuely, T.; Thilgen, C.; Stohr, M.; Diederich, F.; Jung, T. A. *Chem.—Eur. J.* **2008**, *14*, 5794–5802.
(12) Ernst, K. H. *Top. Curr. Chem.* **2006**, *265*, 209–252.
(13) Raval, R. *Chem. Soc. Rev.* **2009**, *38*, 707–721.
(14) Elemans, J.; De Cat, I.; Xu, H.; De Feyter, S. *Chem. Soc. Rev.* **2009**, *38*, 722–736.
(15) Gellman, A. J. *ACS Nano* **2010**, *4*, 5–10.
(16) Lopinski, G. P.; Moffatt, D. J.; Wayner, D. D. M.; Wolkow, R. A. *Nature* **1998**, *392*, 909–911.
(17) De Feyter, S.; Gesquiere, A.; Grim, P. C. M.; De Schryver, F. C.; Valiyaveettil, S.; Meiners, C.; Sieffert, M.; Mullen, K. *Langmuir* **1999**, *15*, 2817–2822.
(18) Bohringer, M.; Morgenstern, K.; Schneider, W. D.; Berndt, R.; Mauri, F.; De Vita, A.; Car, R. *Phys. Rev. Lett.* **1999**, *83*, 324–327.
(19) Ortega Lorenzo, M.; Baddeley, C. J.; Muryn, C.; Raval, R. *Nature* **2000**, *404*, 376–379.
(20) Weckesser, J.; De Vita, A.; Barth, J. V.; Cai, C.; Kern, K. *Phys. Rev. Lett.* **2001**, *87*, 096–101.
(21) Kuehnle, A.; Linderoth, T. R.; Hammer, B.; Besenbacher, F. *Nature* **2002**, 415.
(22) Chen, Q.; Richardson, N. V. *Nat. Mater.* **2003**, *2*, 324–328.
(23) Fasel, R.; Parschau, M.; Ernst, K.-H. *Angew. Chem., Int. Ed.* **2003**, *42*, 5178–5181.
(24) Bluem, M. C.; Cavar, E.; Pivetta, M.; Patthey, F.; Schneider, W.-D. *Angew. Chem., Int. Ed.* **2005**, *44*, 5334.
(25) Fasel, R.; Parschau, M.; Ernst, K.-H. *Nature* **2006**, *439*, 449.
(26) Haq, S.; Liu, N.; Humblot, V.; Jansen, A. P. J.; Raval, R. *Nat. Chem.* **2009**, *1*, 409–414.
(27) Baiker, A. *J. Mol. Catal. A: Chem.* **1997**, *115*, 473–493.
(28) Borszeky, K.; Mallat, T.; Baiker, A. *Tetrahedron: Asymmetry* **1997**, *8*, 3745–3753.
(29) Baddeley, C. J. *Top. Catal.* **2003**, *25*, 17–28.
(30) Sato, I.; Kadowaki, K.; Soai, K. *Angew. Chem., Int. Ed.* **2000**, *39*, 1510–1512.
(31) Mallat, T.; Orglmeister, E.; Baiker, A. *Chem. Rev.* **2007**, *107*, 4863–4890.
(32) Hazen, R. M.; Filley, T. R.; Goodfriend, G. A. *Proc. Natl. Acad. Sci. U.S.A.* **2001**, *98*, 5487–5490.
(33) Hazen, R. M.; Sholl, D. S. *Nat. Mater.* **2003**, *2*, 367.
(34) France, C. B.; Parkinson, B. A. *Langmuir* **2004**, *20*, 2713–2719.
(35) Vidal, F.; Delvigne, E.; Stepanow, S.; Lin, N.; Barth, J. V.; Kern, K. *J. Am. Chem. Soc.* **2005**, *127*, 10101–10106.
(36) Busse, C.; Weigelt, S.; Petersen, L.; Lægsgaard, E.; Besenbacher, F.; Linderoth, T. R.; Thomsen, A. H.; Nielsen, M.; Gothelf, K. V. *J. Phys. Chem. B* **2007**, *111*, 5850–5860.
(37) Weigelt, S.; Busse, C.; Nielsen, M.; Gothelf, K. V.; Lægsgaard, E.; Besenbacher, F.; Linderoth, T. R. *J. Phys. Chem. B* **2007**, *111*, 11342–11345.
(38) Weigelt, S.; Busse, C.; Petersen, L.; Rauls, E.; Hammer, B.; Gothelf, K. V.; Besenbacher, F.; Linderoth, T. R. *Nat. Mater.* **2006**, *5*, 112–117.
(39) Gothelf, K. V.; Brown, R. S.; Thomsen, A.; Nielsen, M. World Patent 2004050231, 2004.
(40) Bombis, C.; Weigelt, S.; Knudsen, M. M.; Nørgaard, M.; Busse, C.; Lægsgaard, E.; Besenbacher, F.; Gothelf, K. V.; Linderoth, T. R. *ACS Nano* **2010**, *4*, 297–311.
(41) Stevens, F.; Dyer, D. J.; Walba, D. M. *Angew. Chem., Int. Ed.* **1996**, *35*, 900–901.
(42) Katsonis, N.; Xu, H.; Haak, R. M.; Kudernac, T.; Tomovic, Z.; George, S.; Van der Auweraer, M.; Schenning, A.; Meijer, E. W.; Feringa, B. L.; De Feyter, S. *Angew. Chem., Int. Ed.* **2008**, *47*, 4997–5001.
(43) Miura, A.; Jonkheijm, P.; De Feyter, S.; Schenning, A.; Meijer, E. W.; De Schryver, F. C. *Small* **2005**, *1*, 131–137.
(44) Hawthorne, F.; Cram, D. J. *J. Am. Chem. Soc.* **1952**, *74*, 5859–5866.
(45) Barluenga, J.; Fañanás, F. J.; Sanz, R.; C., M *Chem.—Eur. J.* **2005**, *11*, 5397–5407.
(46) Schnider, P.; Koch, G.; Prétôt, R.; Wang, G.; Bohnen, F. M.; Krüger, C.; Pfaltz, A. *Chem.—Eur. J.* **1997**, *3*, 887–892.
(47) Lightfoot, A.; Schnider, P.; Pfaltz, A. *Angew. Chem., Int. Ed.* **1998**, *37*, 2897–2899.
(48) Blackmond, D. G.; Lightfoot, A.; Pfaltz, A.; Rosner, T.; Schnider, P.; Zimmermann, N. *Chirality* **2000**, *12*, 442–449.
(49) Menges, F.; Neuburger, M.; Pfaltz, A. *Org. Lett.* **2002**, *26*, 4713–4716.

(50) Menges, F.; Pfaltz, A. *Adv. Synth. Catal.* **2002**, *344*, 40–44.
(51) Loiodice, F.; Longo, A.; Bianco, P.; Tortorella, V. *Tetrahedron: Asymmetry* **1995**, *6*, 1001–1011.
(52) Hansen, T. V.; Skattebøl, L. *Tetrahedron Lett.* **2005**, *46*, 3829–3830.
(53) Llanes-Pallas, A.; Matena, M.; Jung, T.; Prato, M.; Stöhr, M.; Bonifazi, D. *Angew. Chem., Int. Ed.* **2008**, *47*, 7726–7730.
(54) Matena, M.; Llanes-Pallas, A.; Enache, M.; Jung, T.; Wouters, J.; Champagne, B.; Stohr, M.; Bonifazi, D. *Chem. Commun.* **2009**, 3525–3527.
(55) Parschau, M.; Romer, S.; Ernst, K.-H. *J. Am. Chem. Soc.* **2004**, *126*, 15368.
(56) Besenbacher, F.; Lægsgaard, E.; Mortensen, K.; Nielsen, U.; Stensgaard, I. *Rev. Sci. Instrum.* **1988**, *59*, 1035–1038.